

Ursolic Acid Loaded-Mesoporous Hydroxylapatite/ Chitosan Therapeutic Scaffolds Regulate Bone Regeneration Ability by Promoting the M2-Type Polarization of Macrophages

Xijiao Yu^{1,2,*}
Yuxuan Wang^{3,*}
Xiaoliang Liu³
Yuwei Ge^{3,4}
Shanyong Zhang¹

¹Department of Oral Surgery, Ninth People's Hospital, College of Stomatology, Shanghai Jiao Tong University School of Medicine, Shanghai Key Laboratory of Stomatology & Shanghai Research Institute of Stomatology, Shanghai, People's Republic of China; ²Central Laboratory, Department of Endodontics, Jinan Stomatological Hospital, Jinan, Shandong, People's Republic of China; ³Shanghai Key Laboratory of Orthopedic Implants, Department of Orthopedic Surgery, Shanghai Ninth People's Hospital, Shanghai JiaoTong University School of Medicine, Shanghai, People's Republic of China; ⁴Department of Orthopedic Surgery, Shanghai Jiao Tong University Affiliated Sixth People's Hospital, Shanghai, 200233, People's Republic of China

*These authors contributed equally to this work

Correspondence: Yuwei Ge;
Shanyong Zhang
Email geyw2000@163.com;
zhangshanyong@126.com

Purpose: Mesoporous hydroxylapatite (MHAP) might be important for bone regeneration, and ursolic acid (UA) has anti-inflammatory effects. Accordingly, we developed, for the first time, ursolic acid-loaded MHAP-chitosan (MHAP-CS-UA) scaffolds to treat bone defects.

Methods: In vitro, we synthesize biomaterial scaffolds. By SEM, XRD, EDS and FTIR, we test the performance of the hybrid scaffolds. By drug release, flow cytometry, immunofluorescence, alizarin red staining, and Western blotting, we test the anti-inflammatory and osteo-inductive properties of scaffolds. In vivo, we verify osseointegration ability and bone regeneration.

Results: The MHAP is a rod-shaped structure with a length of 100~300nm and a diameter of 40~60nm. The critical structure gives the micro-scaffold a property of control release due to the pore sizes of 1.6~4.3 nm in hydroxyapatite and the hydrogen bonding between the scaffolds and UA drugs. The released UA drugs could notably inhibit the polarization of macrophages to pro-inflammatory macrophages (M1 type) and promote the expression of osteogenic-related genes (COL1, ALP and OPG) and osteogenic-related proteins (BMP-2, RUNX2 and COL1).

Conclusion: The MHAP-CS-UA scaffolds have good anti-inflammatory, osseointegration, osteo-inductivity and bone regeneration. And they will be the novel and promising candidates to cure the bone disease.

Keywords: mesoporous hydroxylapatite, polarization, bone regeneration, ursolic acid, drug delivery

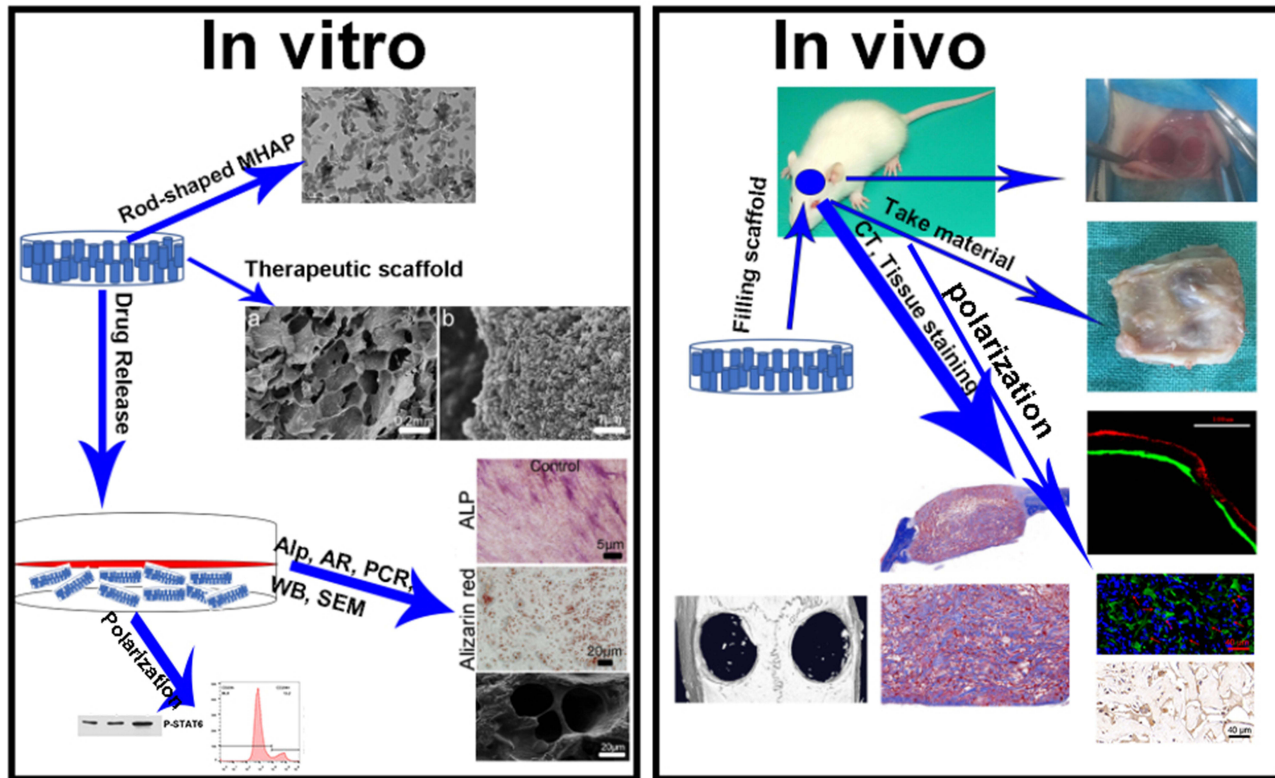
Introduction

Craniofacial bone damage, surgery, infection and bone disease can result in serious bone defects.¹⁻⁴ Such defects bring with them a high economic and spiritual burden to patients.^{5,6} Scientists and trauma surgeons seek many ways to solve these problems, such as xenografts, allografts and autografts.⁷⁻⁹ Good postoperative outcomes are achieved with these procedures. However, donor-site morbidity for autografts and immunogenicity for xenografts and allografts can limit their application.^{10,11} Consequently, additional treatment options for bone defects are urgently needed.

This medical need can also be met with the development of improved bone repair materials that exhibit osteoinductivity, biocompatibility and osteoconductivity.¹²⁻¹⁵ Mesoporous hydroxylapatite (MHAP) is biocompatible and osteoconductive and could



Graphical Abstract



represent such a material.^{16,17} After implantation of hydroxyapatite scaffolds in vivo a carbonated hydroxyapatite layer can form between scaffolds and host bone; however, its osteogenic ability is insufficient for effective repair of bone defects, especially in cases of bone disease.¹⁸ Fortunately, MHAP is also a useful drug delivery system. Its layered porous structure and mesoporous properties provide a large surface area for adsorption of drugs. Further, as an important natural biomaterial, chitosan (CS) is biocompatible and exhibits antimicrobial activity.¹⁹ Functional groups, such as $\sim\text{OH}$ and $\sim\text{NH}_2$ in the CS structure could enhance drug release through hydrogen bond interactions.^{20–22}

Ursolic acid (UA) is a traditional medicinal plant in China that exhibits anti-cancer, anti-inflammatory, anti-virus, anti-bacterial, anti-diabetes, cardiovascular and anti-oxidative properties.^{23–26} Most studies on UA focus on signal transduction pathways, such as transforming growth factor- β /SMAD signal transduction, mitogen-activated protein kinase and nuclear factor κB .^{27,28} Other studies show that UA can increase the expression of osteoblast-specific protein by activating the BMP-2/Smad4 or Wnt/ β -catenin signalling pathway.²⁹

Further, UA is seldom used for anti-inflammatory and osseointegration, to the best of our knowledge.²⁹ Application of UA in hydroxyapatite scaffolds is thus an attractive approach for stimulating bone regeneration and osseointegration.

In this study, MHAP-CS scaffolds loaded with UA (MHAP-CS-UA) were prepared. Initially, MHAP microspheres were prepared with a hydrothermal method using CTAB as an organic template. Next, MHAP-CS porous scaffolds were synthesised by freeze-drying. Finally, UA drugs were loaded into the scaffolds. We found that MHAP-CS-UA scaffolds show good biocompatibility, and drug release from the therapeutic scaffold significantly inhibits the release of inflammatory factors from macrophages, at the same time enhances the expression of osteogenic genes, and accelerates the integration of new bone and material interface and bone regeneration in vivo.

Materials and Methods

Synthesis of MHAP Scaffolds

All chemical reagents were purchased from Sigma. The synthetic process of MHAP scaffolds follows. CTAB,

0.251 mg (mCTAB/(theoretical output $m\text{Ca}_5(\text{PO}_4)_3\cdot\text{OH}$) *100 = 5%) was dissolved in 100 mL deionised water, with stirring for 10 minutes, then placed into a 90°C coil bath. Next, $(\text{NH}_4)_2\text{HPO}_4$ (4.0018 g, 0.03 mol) was dissolved in the CTAB solution, with stirring for 20 minutes at 280 r/min to generate a 0.05 M solution. After 20 minutes, pH of the solution was adjusted to 10.5 with ammonia water.

Separately, 11.9268 g (0.05 mol) $\text{Ca}(\text{NO}_3)_2\cdot 4\text{H}_2\text{O}$ was dissolved in pure water to prepare 100 mL of a 0.3 M solution. The pH of the solution was adjusted to 10.5 with ammonia water. The CTAB solution in the previous step was slowly dripped into this solution over about 40 minutes. The whole process kept the pH of 10.5 unchanged. After mixing solutions, the mixture was stirred for 2 hours at 280 r/min, and then aged at 90°C for 12 hours. Product was washed with deionised water to neutralise and then washed 1 or 2 times with ethanol. Next, it was dried at 80°C for 24 hours, then ground. Finally, the product was calcinated by increasing the temperature by 2°C per minute to 900°C. This temperature was maintained for 4 hours, and the product was allowed to cool naturally to room temperature and then ground again.

Synthesis of MHAP-CS Hybrid Scaffolds

Two grams of CS were dissolved in 50 mL of 2 vol% acetic acid solution (1:25) and stirred mechanically at 320 r/min for 3 hours until completely dissolved. Next, 2 g of MHAP was slowly added to the CS solution, with stirring and dispersing for 2 hours (mass ratio: MHAP:CS = 1:1). The dispersed and uniform solution was transferred to a 24-mesh cell culture medium and placed in the magnetic field of a -20°C refrigerator for 24 hours. The mixture was then cooled to -56°C over the course of about 4 hours and freeze-dried under <10 Pa vacuum. The process took about 96 hours in winter and 72 hours in summer. Product was immersed in 10 wt% NaOH solution for one day, repeatedly washed to a pH of 7. Washing continued for 5 days, with water changes three times a day). Product was then freeze-dried again over about one day. Finally, the preparation of MHAP-CS composite scaffolds was obtained by cutting brittle fracture in liquid nitrogen.

Drug Loading-Release Tests of MHAP-CS-UA Hybrid Scaffolds

Initially, UA powder was dissolved in solvent to create a 1 mg/mL solution. Next, 2.2835 mL of this solution was added to a 50-mL volumetric flask, and anhydrous ethanol

was added to volume to prepare a 100 μmol UA solution. The prepared UA scaffold material (1 μM) is used for sustained drug release. The scaffold material (5 μM , 10 μM) functions as described above.

The release test for MHAP-CS-UA (1 μM , 5 μM , 10 μM) drug scaffold material using immersion of scaffold with the drug in 5.0 mL of phosphate buffer solution (PBS), at normal temperature and an oscillation at 80 rpm. We extracted 1.0 mL of the above solution at different time points (3, 6, 9, 12, 24, 48 and 72 h) while adding back an equal volume of PBS solution. Finally, the corresponding drug concentration was analysed by high-performance liquid chromatography (HPLC, Agilent 1100, US).

Material Characterization

Morphology of MHAP microspheres and MHAP-CS composite scaffolds were examined using scanning electron microscopy (SEM) and characterised by energy dispersive spectroscopy (EDS). The study used transmission electron microscopy to assess nano-mesoporous structures microspheres. Also, the porous structure of MHAP was evaluated with an automatic surface area and porosity analyser at 80 K. Pore size distribution was calculated with the Barrett-Joyner-Halenda method. Phase compositions of MHAP-CS and MHAP-CS-UA composite scaffolds were analysed by X-ray powder diffraction (XRD; D/Max III C, Japan). Finally, Fourier transform infrared spectroscopy was used to identify functional groups on MHAP-CS and MHAP-CS-UA composite scaffolds.

Cell Viability and Attachment

MC3T3-E1 cells were purchased from the Shanghai Institute of Biological Sciences, Chinese Academy of Sciences and human bone marrow mesenchymal stem cells (hBMSCs) from Shanghai Rothen Biotechnology Co., Ltd. (Shanghai, China). Cells were cultured in 10% fetal bovine serum and 1% penicillin/streptomycin medium at 37°C, and 1×10^4 MC3T3-E1 cells were seeded into 96 well plates. After 24 hours, the medium was replaced with MHAP-CS or MHAP-CS-UA scaffold extract. A cell counting kit-8 was cultured for 1 day, 2 days and 3 days. hBMSCs were used as a model to detect adhesion of cells on different scaffolds. Each scaffold was inoculated with 1×10^4 hBMSCs into 24-well plates. hBMSCs were cultured for 12 hours and washed with phosphate. Buffered saline (PBS) with 2.5% glutaraldehyde was added to fix cells. After 20 minutes, hBMSCs were washed three times

with PBS. Samples were dehydrated with increasing ethanol concentrations, 75, 85, 95 and 100%. Finally, the morphology of hBMSCs was characterised by SEM; FEI; Thermo Fisher Scientific, Inc.) on the scaffold with a magnification of 10 kV.

In vitro Tests of Osteogenic Capability

Differentiation of hBMSCs is based on alkaline phosphorylation (ALP, Renbao, Shanghai, China) and alizarin red staining (AR, Sigma-Aldrich). 1×10^4 hBMSCs were inoculated into 24-well plates. After 24 hours, medium was replaced with medium containing MHAP-CS, MHAP-CS-UA scaffolds. After 7 and 14 days of culture, hBMSCs were immobilised with 4% paraformaldehyde. Fixed cells were washed three times with PBS and stained with ALP and AR kits. Residual substance was washed out with PBS. Finally, stained samples were photographed by an inverted phase-contrast microscope.

The expression levels of osteogenesis-related genes and macrophage polarization marker genes, including alkaline phosphorylation (ALP), collagen 1 (COL1) and osteoprotegerin (OPG) were detected by real-time quantitative polymerase chain reaction RT-PCR. 4×10^6 MC3T3-E1 cells were seeded in a 6-well plate containing the extract of the above scaffold material. Seven days later, total RNA was collected using a RNeasy Mini kit (Qiagen, Inc., Valencia, CA, USA) and reverse transcribed into cDNA (Takara Bio, Inc., Otsu, Japan). An SYBR Premix Ex Taq kit (Takara Biotechnology Co., Ltd.) and an ABI 7500 Sequencing Detection System (Applied Biosystems; Thermo Fisher Scientific, Inc.) was used to perform qPCR. Glyceraldehyde-3-phosphate dehydrogenase (GAPDH) gene expression was used as a standard reference, the following thermocycling conditions were used: 40 cycles of denaturation at 95°C for 5 s and amplification at 60°C for 24 s. Data were quantified with the $2^{-\Delta\Delta Ct}$ method. All the above steps are in accordance with the instructions of the reagent manufacturer. The PCR primers were:

GAPDH forward 5'-CACCACCATGGAGAAGGC CG-3'

and reverse 5'-ATGATGTTCTGGGCAGCCCC-3'

OPG forward 5'-CGAGCGCAGATGGATCCTAA-3'

And reverse 5'-CCACATCCAACCATGAGCCT-3'

Col1 forward 5'- GCTCCTCTTAGGGGCCACT-3'

And reverse 5'- CCACGTCTCACCATTGGGG-3'

ALP forward 5'- CATCATCATGTTCTGGGAG-3'

And reverse 5'- GACCTGAGCGTTGGTGTGT-3'

MC3T3-E1 cells were cultured in the medium with MHAP/CS or MHAP-CS-UA scaffolds to measure the expression of osteoblast-related proteins (BMP-2, COL1, RUNX2, Smad1/5). Raw 264.7 culture method was similar to the above. The antibodies were Arg-1, CD206 and P-STAT from CST. Protein was extracted from the radio-immunoprecipitation assay (RIPA) lysis buffer (cat. no. C500005; Sangon Biotech Co., Ltd.) containing 1 μ M protease inhibitor. Then centrifuge at a speed of 12,000 rpm for 10 minutes. The bicinchoninic acid assay (BCA) was used to measure corresponding protein concentration. Gel electrophoresis was carried out with SDS-PAGE and transferred to PVDF membranes and blocked with 5% milk for 1 hour. Membranes and primary antibody were incubated overnight at 4 degrees. Membranes were washed with PBS three times and incubated with a second antibody coupled with horseradish peroxidase for 1 hour. Finally, horseradish peroxidase-conjugated secondary antibodies reactivity was detected using the Odyssey infrared imaging system (LI-COR Biosciences, Lincoln, NE, USA).

Flow Cytometry

Raw 264.7 seeds at a density of 4×10^5 seeded in 6 well plates. By flow cytometry, macrophage subpopulation markers CD16/32 (M1) and CD206 (M2) for the assessment of different phenotypes. The Mouse CD16/32 PE and the Mouse CD206 Alexa 647 were incubated separately according to the manufacturer's instructions. Finally, they were analysed on a Guava flow cytometer (Millipore). Data were analysed using guavaSoft 3.1.1 software.

In vivo Tests of Osteogenic Capability

The Animal Research Committee of the Ninth People's Hospital Affiliated to the Medical College of Shanghai Jiao Tong University approved all animal experiments, and followed with national standard GB/T 35892-2018 "Laboratory animal—Guideline for ethical review of animal welfare". In the process of performing animal experiments, all operations related to animal welfare and treatment are carried out in accordance with the "Chinese Animal Management Regulations" promulgated by the National Science and Technology Commission of the People's Republic of China. Fifteen Sprague-Dawley female rats (200-250 g) were selected. A bilateral critical size skull defect model was used to evaluate bone regeneration. The diameter and height of bone defects were 5 mm and 2 mm, respectively. MHAP-CS and MHAP-CS-UA stents (n = 5)

were filled in the defect area, and the scalp was sutured. Multicolour continuous fluorescence labelling was used to characterise the formation and mineralisation of new bone. AR (30 mg/kg, Sigma-Aldrich) and calcein (30 mg/kg, Sigma-Aldrich) were injected intraperitoneally to label the animals three and 21 days before euthanasia. Animals were euthanised after twelve weeks. The bilateral critical size skull defects were isolated from the surrounding tissues. Samples were immersed in formalin solution buffered by 4% phosphate for 7 days, and then assessed with a micro CT system (Skyscan 1072; Skyscan, Aartselaar, Belgium). The parameters are set to 90 KV voltage, 88 uA current and 28 um voxel size. After scanning, 3D images were reconstructed. Bone healing was evaluated by calculating bone mineral density (BMD) and new bone mass/tissue volume (BV/TV). Undecalcified samples were embedded in polymethyl methacrylate. The sagittal section of the skull was cut 150 mm thick with a slicer (Leica, Hamburg, Germany). Multicolour continuous fluorescence labelling (Leica, Heidelberg, Germany; alizarin red: 543/580–670 nm, calcein: 488/500–550 nm) was observed with confocal laser scanning microscopy. The mineralisation rate was quantified by brightness analysis based on different colour bands. Soft tissue around the skull was removed and immersed in 10% EDTA for 30 days, then embedded in paraffin. Histological sections were prepared for Masson staining, immunohistochemistry and immunofluorescence for IL-1beta, IL-6, TNF-alpha, Inos, Arg-1, BMP-2, COL-1, RUNX2 and OPG protein expression. Finally, sections were examined using light microscopy (magnification, $\times 10$). Images were analysed using Image-Pro Plus 6.0 (Media Cybernetics, Inc., Rockville, MD, USA).

Statistical Analysis

All data were expressed as means \pm standard deviation (SD) and were analysed using one-way ANOVA. $*p < 0.05$ was considered statistically significant.

Results and Discussion

Morphologies and Structures of MHAP Nanoparticles

As shown in Figure 1A and B, MHAP was a short rod-like structure with a length of 100–300 nm and a diameter of 40–60 nm. Figure 1C shows the N₂ adsorption-desorption isotherms of the MHAP nanoparticles. The mesopore sizes were mainly distributed at approximately 2.2–23.3 nm, pore size distribution was calculated with the Barrett–

Joyner–Halenda method (Figure 1D). The mesoporous structure of MHAP nanoparticles provided good basic conditions for material degradation and drug loading. MHAP had great application potential as an engineering material for bone tissue repair, but its osteo-inductivity and osseointegration needed to be improved, so as to better meet the clinical needs.^{30–32} Considering that MHAP had the ability to load drugs, we chose to load UA into it. The UA drug was extracted from many plants such as the whole grass of the Labiatae plant, *Prunella vulgaris*, and the leaves of the holly, holly, iron holly leaves.³³ The UA is a triterpenoid compound found in natural plants and has many biological effects such as sedative,³⁴ anti-inflammatory,³⁵ antibacterial,³⁶ and immune defense responses.³⁷ The Ursolic acid (UA), also promote osteoblast differentiation and new bone formation.

Morphology and Structures of MHAP-CS Hybrid Scaffolds

If the usual mode of administration, such as oral or intravenous, is used, the biological activity of the drug may be difficult to achieve maximum efficiency. Here, we first created the MHAP-CS-UA composite scaffold as the drug delivery system for UA. The MHAP-CS scaffold was prepared by freeze-drying using MHAP nanoparticles and CS as raw materials. Interestingly, MHAP-CS scaffolds exhibited a three-dimensional interconnected macroporous structure with pore sizes of 100–300 μm (Figure 2A). Surfaces of the scaffolds were inlaid with many evenly distributed rod-like structures of MHAP powder (Figure 2B and C). The Ca, and P elements originated from MHAP nanoparticles; the C element originated from CS; the O element originated from both MHAP and CS. C element distribution images are shown in Figure 2D, Ca element distribution images in Figure 2E, O element distribution images in Figure 2F, and P element distribution images in Figure 2G. An electron microscope scan image of the surface of the MHAP-CS scaffold is also included (Figure 2H). A merged image of the above elements was prepared (Figure 2I).

EDS of the MHAP-CS hybrid scaffolds indicated that the main chemical elements included C, Ca, O and P (Figure 2J). XRD patterns and the FTIR spectra of MHAP nanoparticles, CS powders, MHAP-CS and MHAP-CS-UA hybrid scaffolds are provided in Figure 2K and L. MHAP-CS and MHAP-CS-UA contained MHAP diffraction peaks. CS was a semi-crystalline material, and its

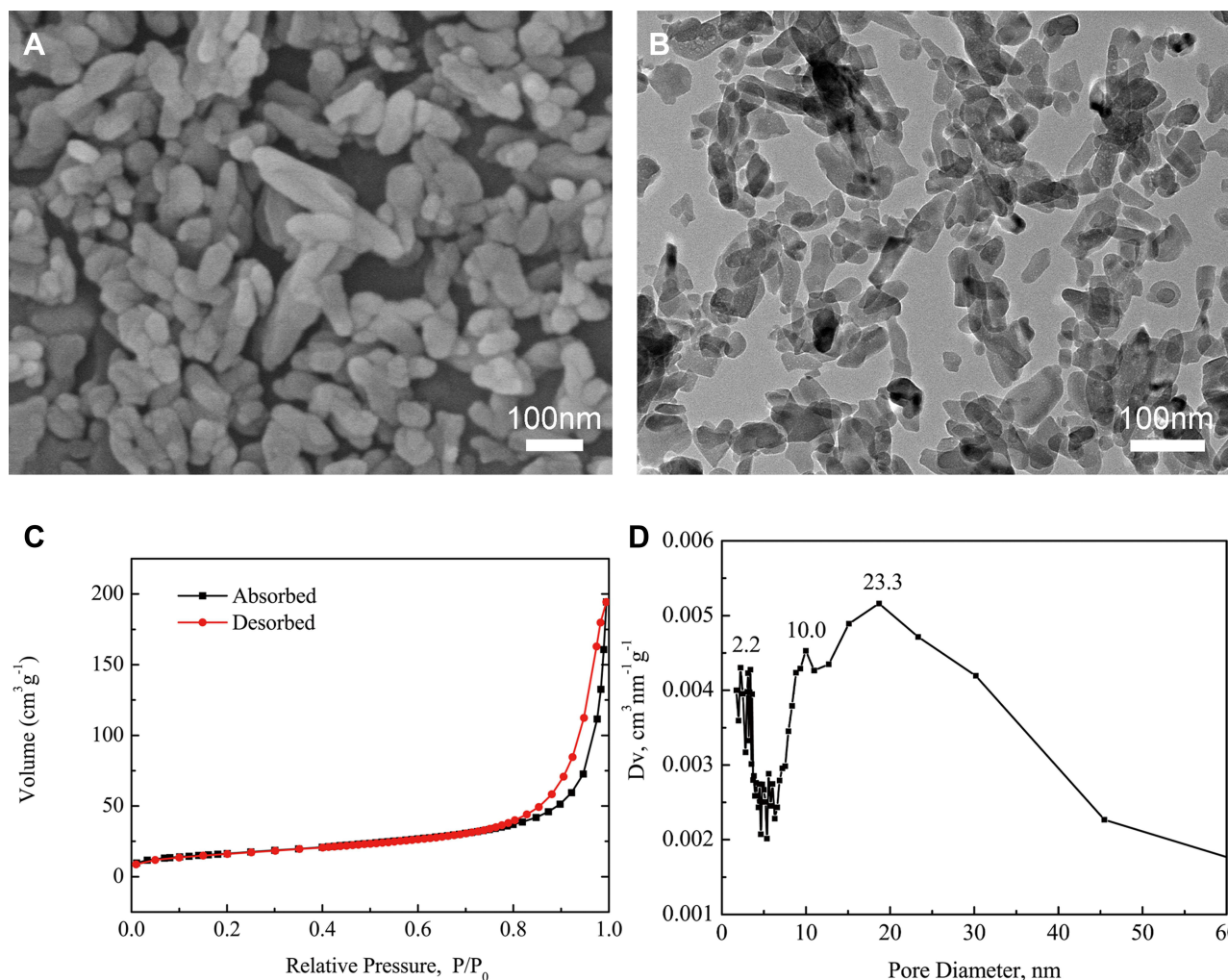


Figure 1 Characterization of MHAP nanoparticles: (A) SEM image; (B) TEM image; (C) N₂ adsorption-desorption isotherms; and (D) BJH pore size distribution curve.

diffraction peak was located at $2\theta = 28.01^\circ$. Moreover, FTIR spectra indicated an OH group located at around 3440 cm^{-1} . For the CS powders, MHAP-CS and MHAP-CS-UA scaffolds, the band at about 2920 cm^{-1} corresponded to CH₂ and CH stretching vibrations. The band at 1550 cm^{-1} was assigned to N-H bending vibration. Bending vibrations of phosphate (PO₄³⁻) groups were located at 566 and 602 cm^{-1} , and bands due to stretching vibrations were located at 1093 and 1031 cm^{-1} . The band at 1384 cm^{-1} is an interference peak of the instrument.

Drug Release Property of MHAP-CS-UA Therapeutic Scaffolds

The MHAP-CS scaffold has outstanding performance as a carrier, which is mainly related to its special structure. The MHAP-CS composite scaffold has interconnected macroporous structure with pore sizes of approximately

$100\sim 300\text{ }\mu\text{m}$, which were originated from the sublimation of frozen solvent during the freeze-drying process (Figure 2A). These mesoporous structures are the locations where the drug is loaded. In addition, within the MHAP nanoparticles, N₂ adsorption-desorption isotherms proved the existence of mesopores in MHAP nanoparticles. The mesopore size is mainly distributed in about $2.2\sim 23.3\text{ nm}$. The mesoporous structure of MHAP nanoparticles provided good basic conditions for material degradation and drug loading (Figure 1). MHAP nanoparticles are widely and evenly distributed in the scaffold material (Figure 2B and C). In addition, many of the polar functional groups present in the MHAP-CS composite scaffold can adsorb drug molecules on the surface of the scaffold by hydrogen bonding, thereby achieving controlled drug release (Figure 2K and L). Therefore, we design different concentrations of scaffold materials for drug release experiments.

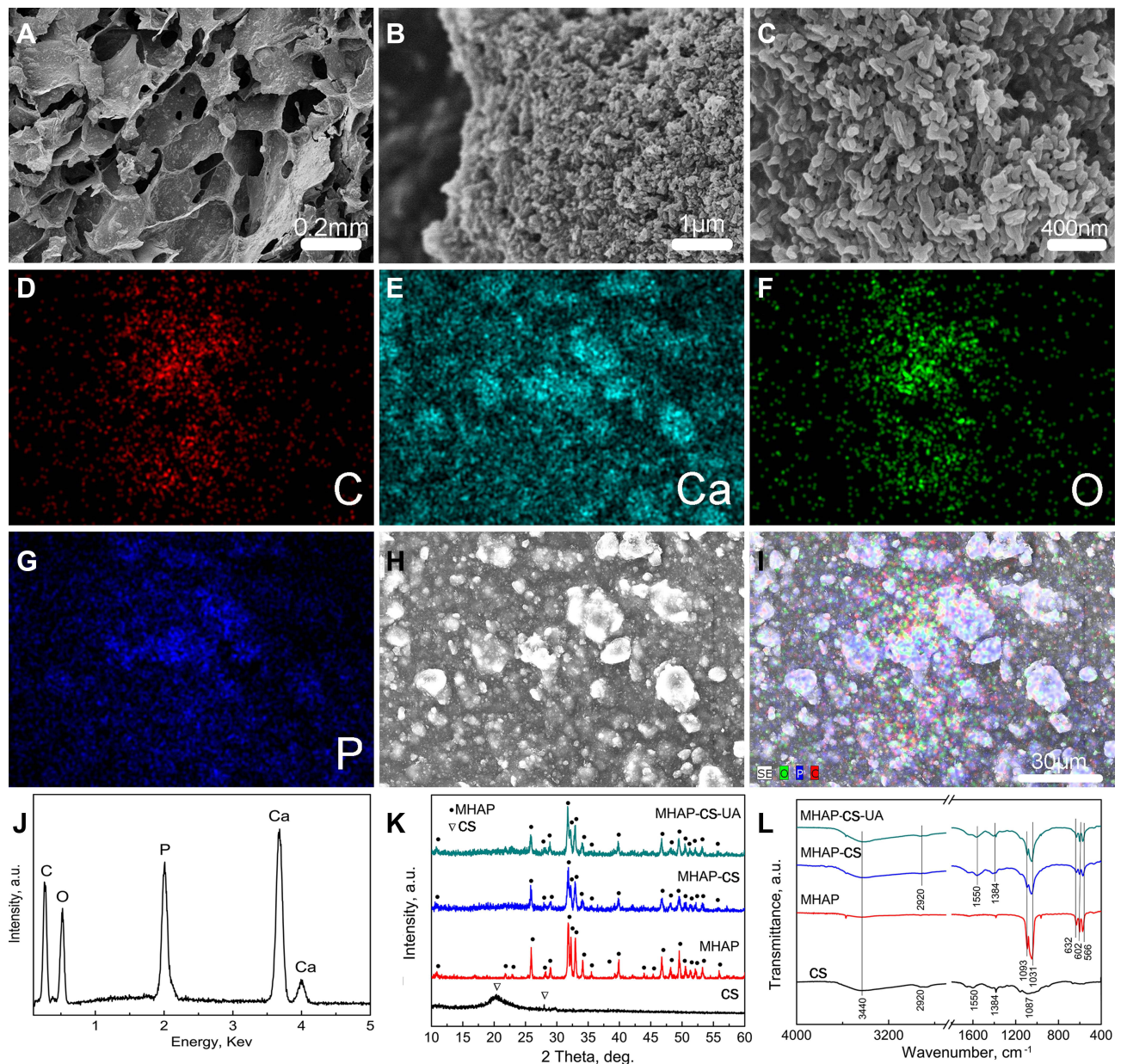


Figure 2 (A) Low-resolution SEM image; (B and C) high-resolution SEM image; (D–I) C, Ca, O and P element distribution image; (J) EDS pattern; (K) XRD patterns and (L) FTIR spectra of MHAP nanoparticles, CS powders, MHAP-CS and MHAP-CS-UA hybrid scaffolds.

Different concentrations of UA and MHAP-CS were made into composite scaffolds with different drug concentrations. In the drug release test, MHAP-CS-UA (1µM), MHAP-CS-UA (5µM) and MHAP-CS-UA (10µM) were immersed in PBS, and the corresponding drug concentrations were determined by high performance liquid chromatography. Characterization. All samples showed similar drug release trends (Figure 3A). The UA drug is rapidly released from the drug carrier within 24 hours, and the release rate begins to decrease over time. After 72 hours, the UA drug concentrations released from MHAP-CS-UA

(1µM), MHAP-CS-UA (5µM), and MHAP-CS-UA (10µM) reached 0.033µM, 0.171µM, and 0.342µM, respectively (Figure 3B–D).

In vitro Cytocompatibility and Osteo-Inductivity of MHAP-CS-UA Therapeutic Scaffolds

We applied proliferation and cell adhesion assays to detect the biocompatibility of MHAP-CS-UA scaffolds. The proliferation ability of the cells was examined by

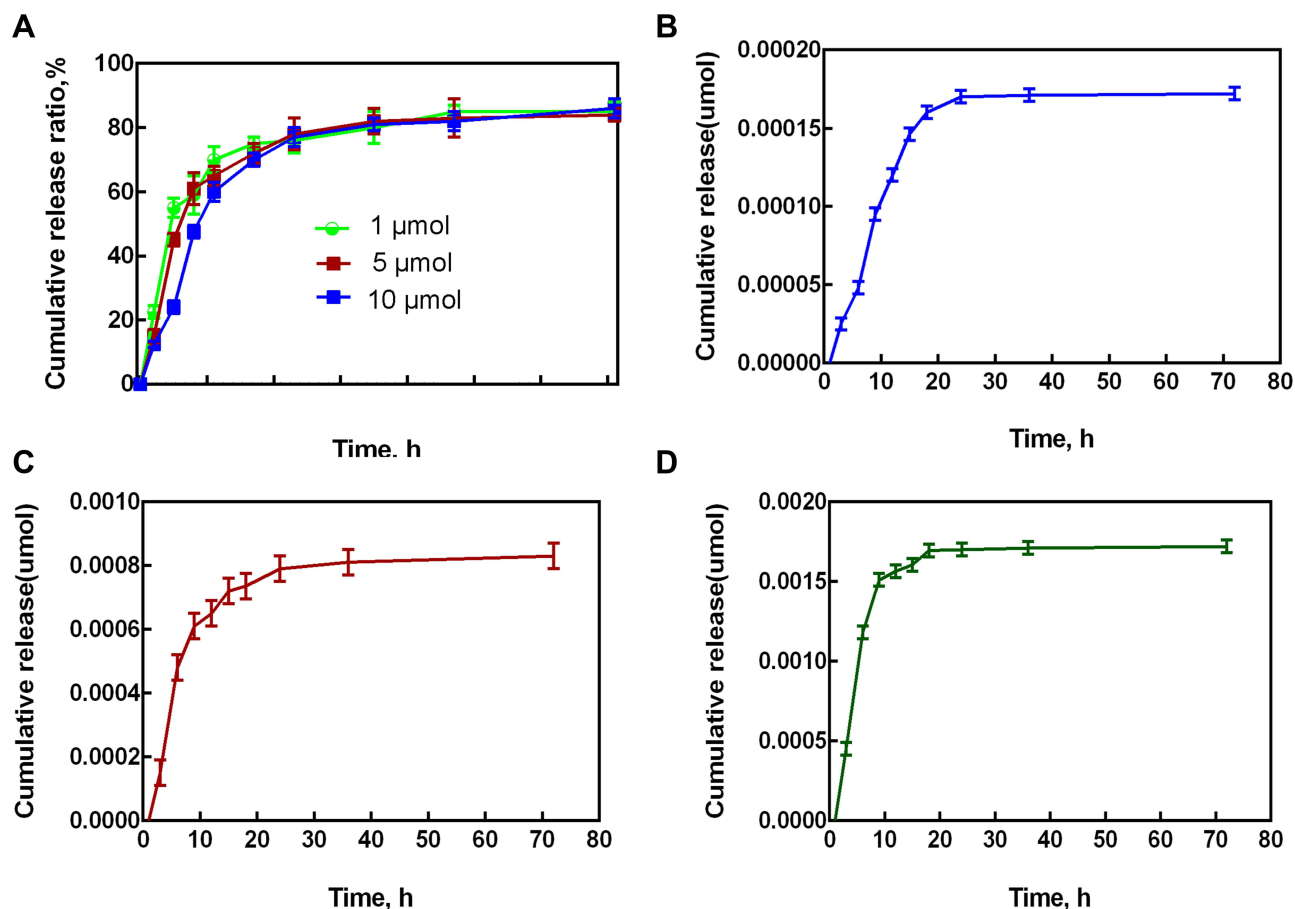


Figure 3 The release of drugs at different concentrations. (A) The cumulative drug release ratios for different MHAP-CS-UA scaffolds. (B) MHAP-CS-UA (1μM), (C) MHAP-CS-UA (5μM) and (D) MHAP-CS-UA (10μM).

co-culture with MC3T3-E1 cells using different concentrations of samples. The results obtained by the CCK-8 method (Figure 4A) showed that the all groups were active. This result demonstrates that the UA released by the MHAP-CS-UA treatment scaffold is less toxic to MC3T3-E1 cells. However, they could promote the proliferation of MC3T3-E1 cells. By scanning electron microscopy, we found that hBMSC was evenly distributed on the MHAP-CS and MHAP-CS-UA scaffold (Figure 4D), indicating that the MHAP-CS-UA scaffold has excellent cell compatibility.

Alkaline phosphatase essential for early bone formation and is a major component of extracellular matrix mineralisation. Uptake of calcium into nodules is also a sign of bone mineralisation. ALP staining and AR staining images of hBMSCs after 7 days and 21 days of treatment in the blank control group, MHAP-CS and MHAP-CS-UA groups is shown in Figure 4B and C. The order of the osteogenesis and bone mineralisation ability shown in these three groups is MHAP-CS-UA > MHAP-CS > and blank.

The expression levels of the ALP, RUNX2 and COL1 proteins were analysed using MHAP-CS and control scaffolds as controls group to evaluate the osteoinductive effect of the MHAP-CS-UA scaffold (Figure 4E). The results showed that the expression of osteogenic related proteins was upregulated compared to the control group. In addition, the MHAP-CS-UA group also exhibited higher levels of expression of P-Smad1/5 than the control group. Similar results were obtained at the gene level (Figure 4F–H), and expression levels of ALP, COL1 and OPG in the MHAP-CS-UA group were upregulated compared to control and the MHAP-CS group.

In vitro Activate the Polarization of M2 Macrophages of MHAP-CS-UA Therapeutic Scaffolds

Figure 5A–H shows the polarization of macrophages mediated by different processing factors by using flow cytometry. Figure 5A, b, c respectively represented

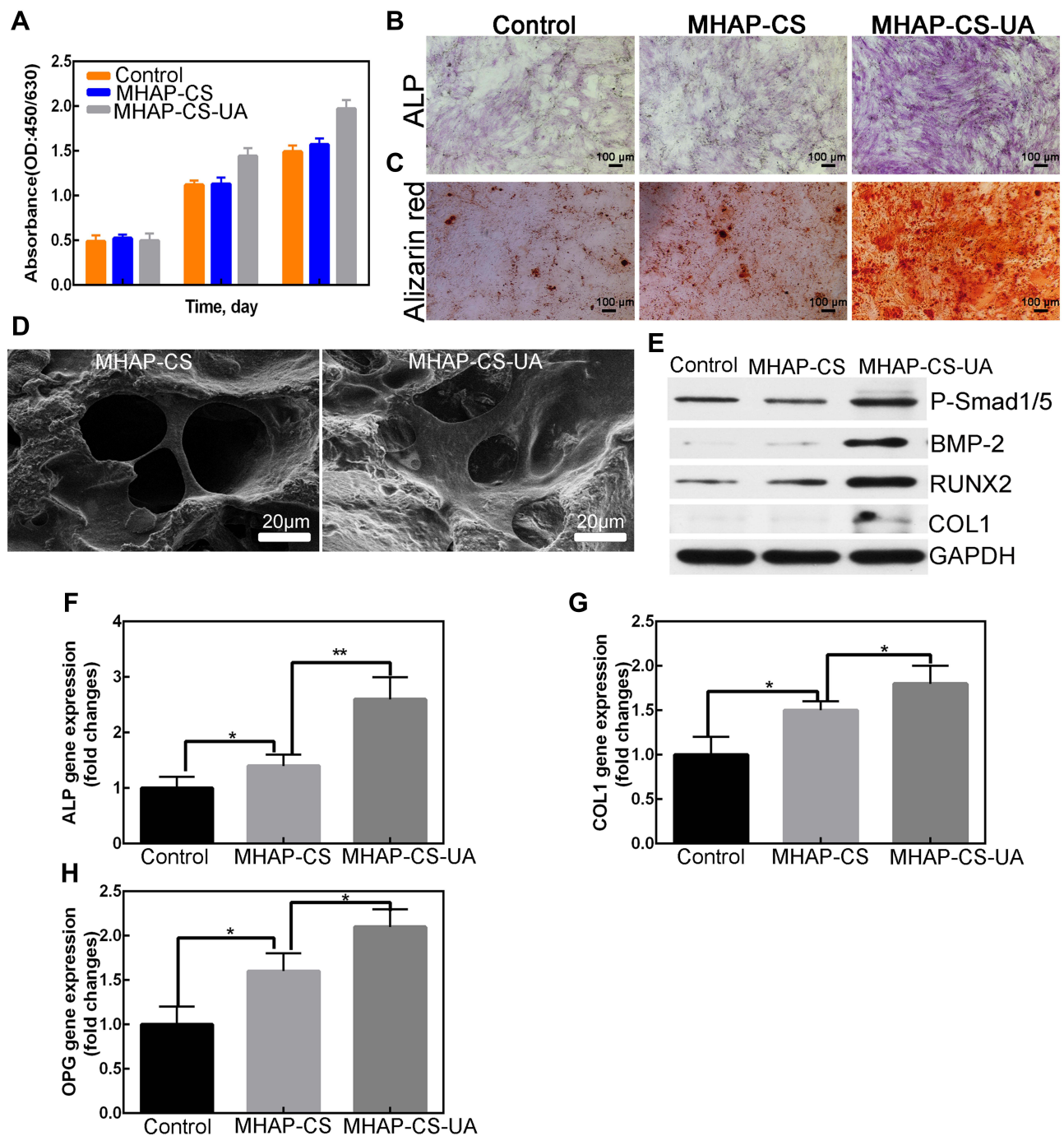


Figure 4 In vitro osteo-induction experiments on scaffolds. **(A)** CCK-8; **(B and C)** ALP staining and alizarin red staining; **(D)** scanning electron microscope (SEM) of scaffolds; **(E)** detect protein expression level by Western blot; **(F–H)** detect gene expression level by PCR. * $P < 0.05$, ** $P < 0.01$.

Control (LPS), MHAP-CS (LPS+MHAP-CS extract) and MHAP-CS (LPS+MHAP-CS-UA extract). From the results of statistical analysis, UA released from the scaffold material obviously inhibited the process of macrophages polarization to M1 type (Figure 5D). Figure 5E–H show that the MHAP-CS-UA scaffold

material promote the differentiation of macrophages into M2 type. By Western blot, MHAP-CS-UA scaffold activated the polarization of M2 macrophages by activating the P-STAT6 signaling pathway (Figure 5I–L).

To summarize the in vitro experiments, UA released from the MHAP-CS-UA scaffold activated the polarization

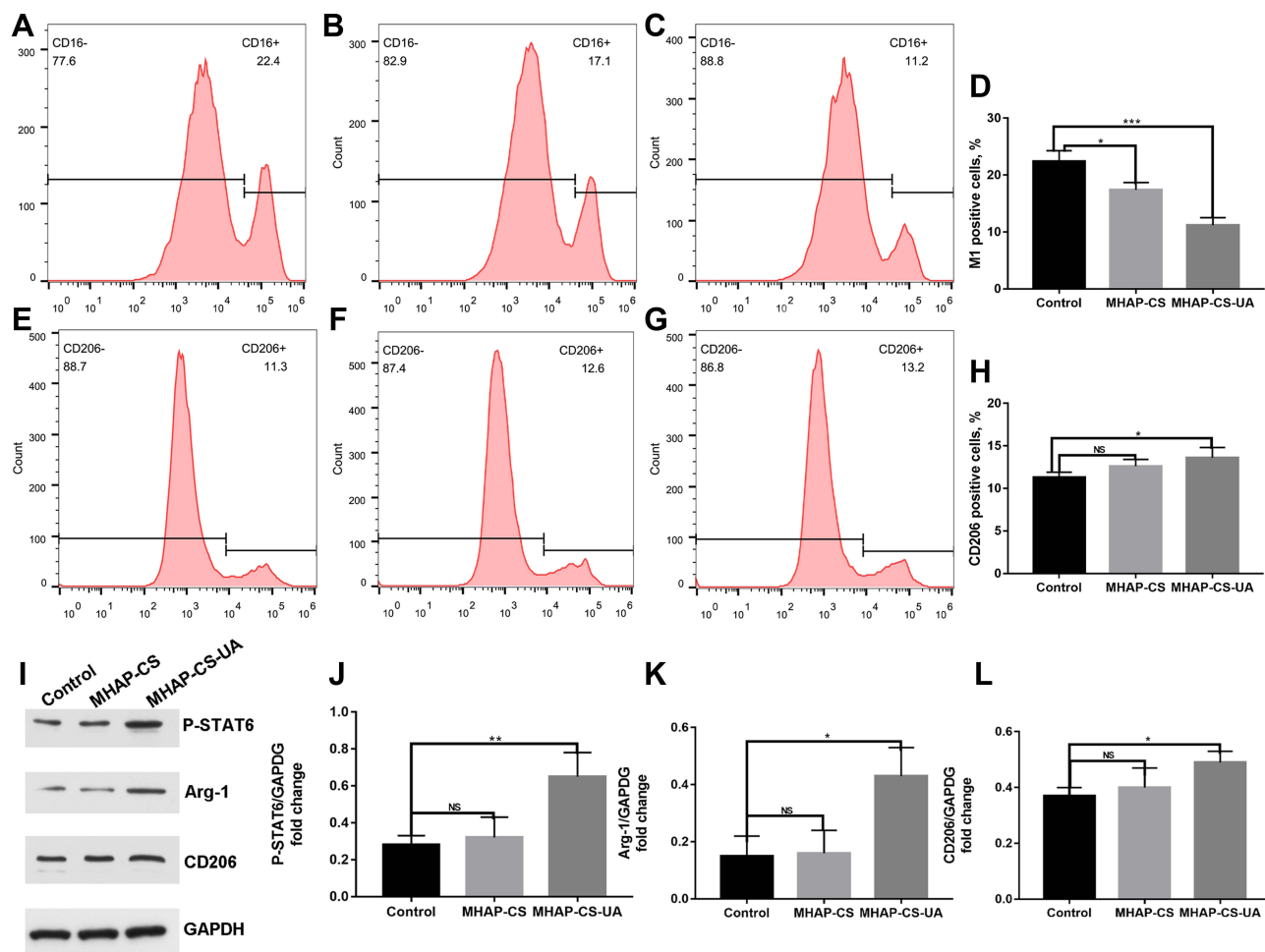


Figure 5 In vitro MHAP-CS-UA therapeutic scaffold regulates macrophage polarization. (A–C) Control (LPS), MHAP-CS (LPS+MHAP-CS extract) and MHAP-CS (LPS+MHAP-CS-UA extract) were flow cytometry maps that inhibit the polarization of M1 macrophages. (D) The above statistical analysis. (E–G) Control (IL-4), MHAP-CS (IL-4+MHAP-CS extract) and MHAP-CS (IL-4+MHAP-CS-UA extract) were flow cytometry maps that promoted the polarization of M2 macrophages. (H) The above statistical analysis. (I–L) Detect M2 macrophages protein expression level by Western blot. * $P < 0.05$, ** $P < 0.01$, *** $P < 0.001$, ns- not significant.

of M2 macrophages by activating the P-STAT6 signaling pathway. M2 type macrophages had anti-inflammatory effects and could produce anti-inflammatory factors, such as IL-10 and arginase 1 (Arg-1). And it would promote the integration of bone and material. When the scaffold was filled on the surface of the bone defect, the macrophages would accumulate to activate the immune response, promote the polarization of the macrophages to the M1 type, and release inflammatory factors. At this time, the release of UA in the scaffold material could inhibit the polarization process of M1 macrophages.

Next, the MHAP-CS-UA scaffold entered the bone repair process. ALP staining and AR staining confirm that the MHAP-CS-UA composite scaffold exhibits superior ability to promote osteoblast differentiation (Figure 4B). Specific protein expression related to osteoblast differentiation was significantly upregulated by the

MHAP-CS-UA composite scaffold (Figure 4E). Moreover, UA can also play a role in the regulation of bone formation via the BMP-2/Smad1/5 and the Wnt/ β -catenin signalling pathways. Further, the expression of BMP-2 and P-Smad1/5 is higher in MHAP-CS-UA than in MHAP-CS. Similar results were verified for RUNX-2 and COL1.

In vivo Bone Regeneration Property of MHAP-CS-UA Therapeutic Scaffolds

The MHAP-CS-UA scaffold was evaluated for bone regeneration by establishing a rat skull defect model (Figure 6). Three-dimensional reconstruction of CT images showed that after 12 weeks of establishment of the rat skull defect model, no new bone formation was observed in the blank control group and some new bone formation was evident in the MHAP-CS and MHAP-CS-UA groups (Figure 6A).

Quantitative results show that MHAP-CS-UA has an increase in volume and density of new bone formation compared to MHAP-CS (Figure 6B). In addition, different bone mineral density (BMD) values were detected in the

three groups in the following order: MHAP-CS-UA group > MHAP-CS group > blank group (Figure 6C).

Micro-CT showed that the bone regeneration ability was significantly enhanced in the MHAP-CS-UA group.

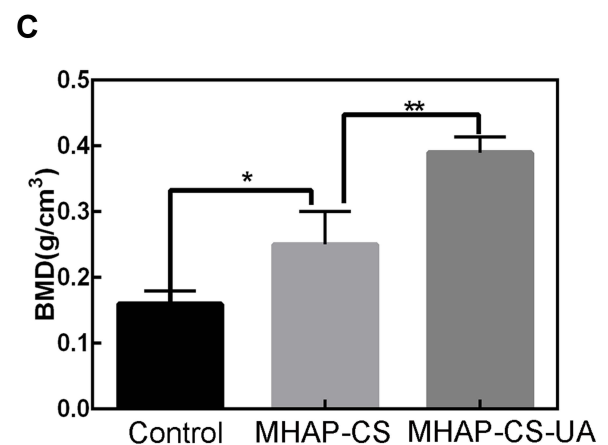
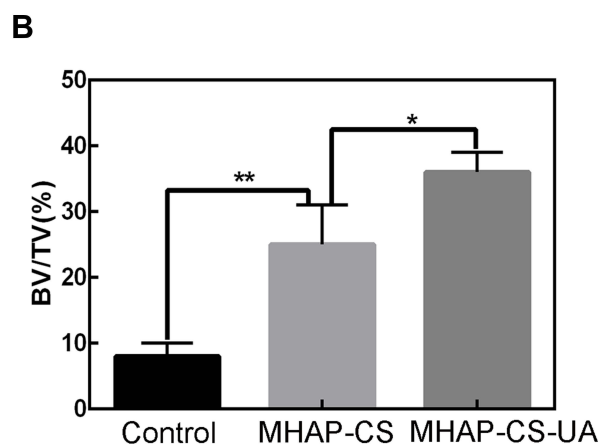
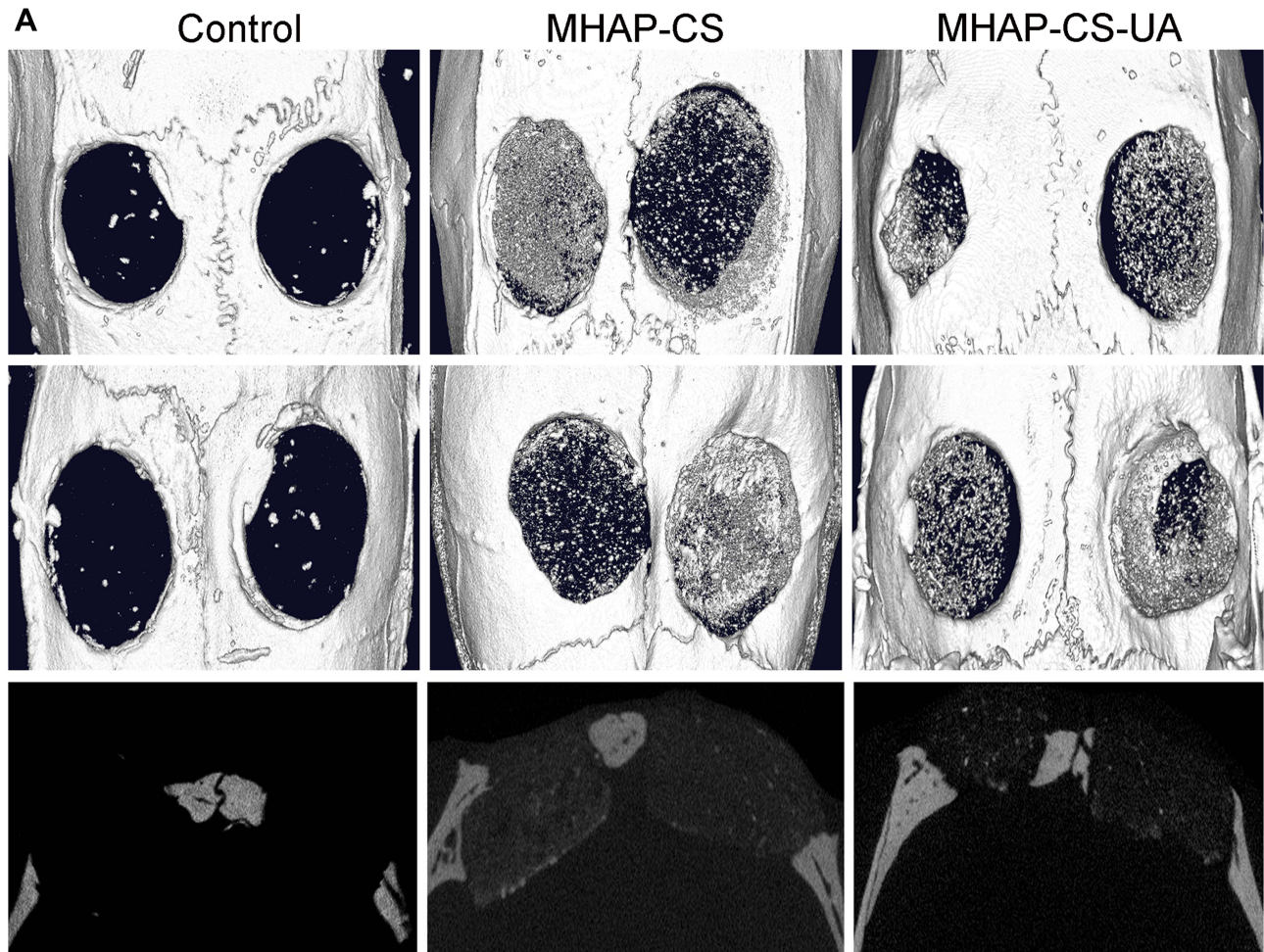


Figure 6 In vivo osteogenic activity of scaffolds. (A) Micro-CT images of calvarial defects model; (B) new-bone volume/tissue volume (BV/TV); (C) morphometric analysis of bone mineral density (BMD). * $P < 0.05$, ** $P < 0.01$.

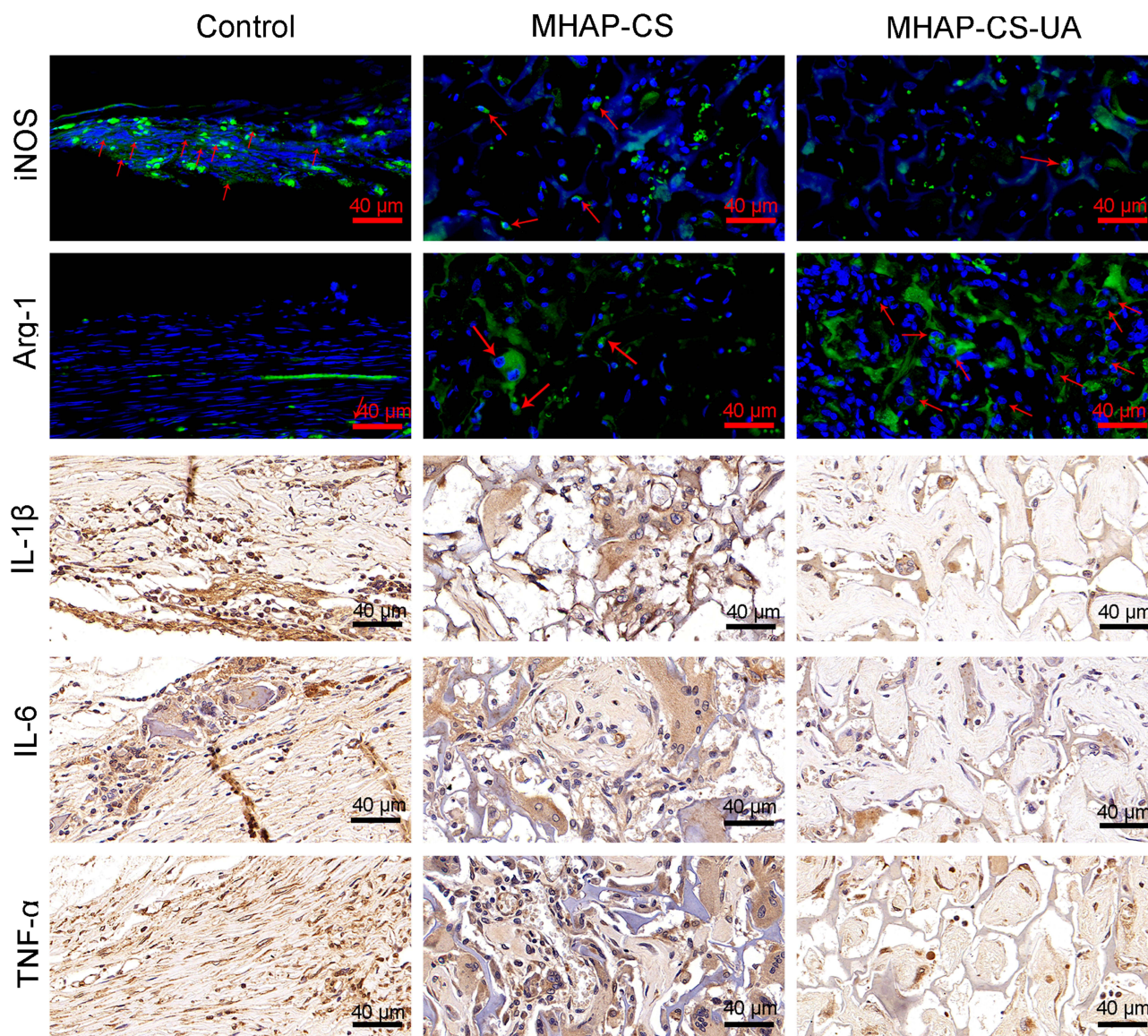


Figure 7 By immunofluorescence and immunohistochemistry, observed iNOS, Arg-1, IL-1 β , IL-6 and TNF- α in the control group, MHAP-CS group and MHAP-CS-UA group. The first row of red arrows represents the iNOS protein, and the second row of red arrows represents the Arg-1 protein.

Next, we considered whether the macrophages in the material also changed. Therefore, we did immunofluorescence and immunohistochemistry. The immunofluorescence of iNOS and Arg-1 proteins in tissue sections under different groups are shown in Figure 7. Compared to the control group, the expression of iNOS in the MHAP-CS-UA group was significantly inhibited. While the expression of Arg-1 in the MHAP-CS-UA group was significantly increased. Next, we continue to do immunohistochemical experiments on inflammatory factors on the above sections. Compared to the control group, the expression of IL-1 β , IL-6 and TNF- α in the MHAP-CS-UA group were also significantly inhibited.

Histomorphometry of new bone formation and mineralization with alizarin red and calcein fluorescence showed that the average distance between the MHAP-CS and MHAP-CS-UA groups were greater than that of the control group (Figure 8A and B). The above conclusions confirmed that the mineralization rate of the MHAP-CS-UA group ($6.12 \pm 0.21 \mu\text{m}/\text{day}$) was higher than that of the vehicle group ($4.24 \pm 0.25 \mu\text{m}/\text{day}$) and the blank group ($2.11 \pm 0.16 \mu\text{m}/\text{day}$). In addition, Masson staining showed that the blank group showed a large amount of fibrous tissue and a small amount of newly formed bone around the defect site, while the MHAP-CS-UA and MHAP-CS scaffold were more collagen and new bone formation

(Figure 8C). Compared with the MHAP-CS group, the new group had more new bone, suggesting that the released UA can promote the mineralization of the osteogenic tissue.

Osteoblast-associated protein expression in scaffold materials was detected by immunohistochemistry. We performed immunohistochemistry using tissue sections from each of the control group, MHAP-CS group and MHAP-CS-UA group (Figure 8D). The osteogenic related proteins (OPG, RUNX-2, COL1, BMP-2) were detected. We found that the expression of MHAP-CS-UA proteins (OPG, RUNX-2, COL1, BMP-2) were significantly higher than that of the MHAP-CS group. In addition, protein expression in the MHAP-CS group was also significantly enhanced compared to the control group. This further

showed that MHAP-CS-UA would promote bone repair by releasing UA.

Conclusion

The schematic diagram of the entire manuscript is shown in graphical abstract. In summary, the concept behind MHAP-CS-UA treatment scaffolds are: (i) synthesis of a mesoporous MHAP scaffold; (ii) use of this scaffold for preparation of a drug carrier, MHAP-CS; (iii) formation of a drug-loaded MHAP-CS-UA that regulates the polarization of macrophages by activating the P-STAT6 signaling pathway, and then transition to the process of bone regeneration. A porosity of $\sim 100 \mu\text{m}$ promotes regeneration of collagen and differentiation of new bone tissue. Hydrogen bonding between the mesoporous

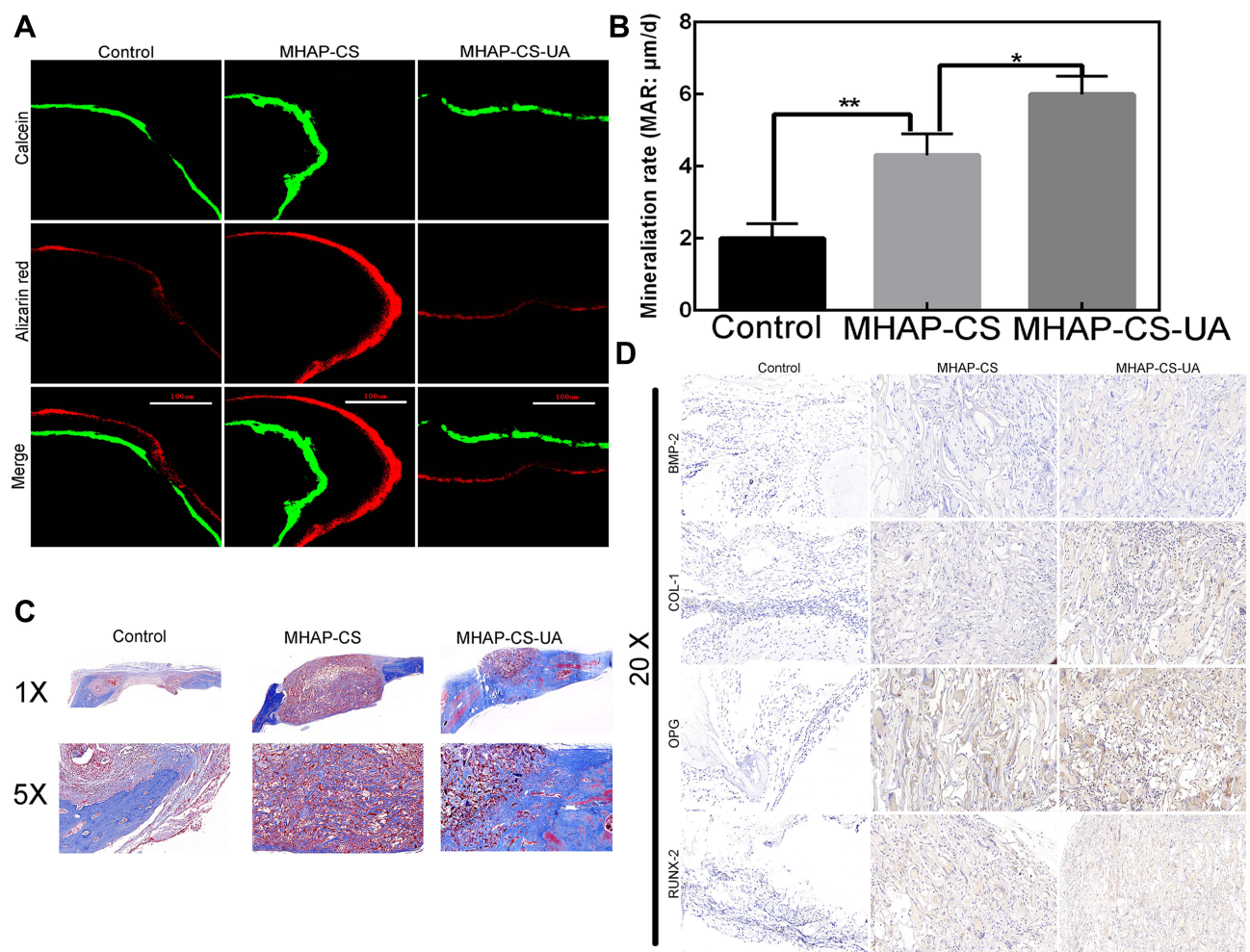


Figure 8 (A) The green and red lines represent the 3 weeks and 3 days before euthanasia, respectively. The last line is the merged images; (B) mineralization rate (the average distance between two lines divided by the number of days); (C) by Masson's trichrome staining, histomorphological analysis for determining newly formed bones (blue) and collagen components (red). (D) By immunohistochemistry, observed BMP-2, COL 1, OPG and RUNX-2 in the control group, MHAP-CS group and MHAP-CS-UA group. * $P < 0.05$, ** $P < 0.01$.

structure and polar group in the scaffold enhances the controlled release of UA. UA in the vector significantly enhances the expression of genes and proteins related to new bone formation and differentiation. The rat skull defect model extends findings to in vivo realm. Therefore, the MHAP-CS-UA treatment exhibits overall good performance. It is important for stimulating osteogenic differentiation and new bone regeneration after injury or for treatment of disease.

Acknowledgments

This work was supported by the Dean's Research Fund of Jinan Stomatological Hospital (202102).

Disclosure

The authors declare no conflicts of interest in this work.

References

- Aghaloo TL, Chaichanasakul T, Bezouglaia O, et al. Osteogenic potential of mandibular vs. long-bone marrow stromal cells. *J Dental Res.* 2010;89:1293–1298.
- Bai X, Lu S, Liu H, et al. Polysaccharides based injectable hydrogel compositing bio-glass for cranial bone repair. *Carbohydrate Polymers.* 2017;175:557–564.
- Sumathra M, Sadasivuni KK, Kumar SS, Rajan M. Cisplatin-Loaded Graphene Oxide/Chitosan/Hydroxyapatite Composite as a Promising Tool for Osteosarcoma-Affected Bone Regeneration. *ACS Omega.* 2018;3:14620–14633. doi:10.1021/acsomega.8b02090
- Tao J, Zhang Y, Shen A, et al. Thermosensitive Hydrogel/Nanoparticle-Loaded System for Local Delivery of Vancomycin in the Treatment of Osteomyelitis. *Int J Nanomed.* 2020;15:5855–5871. doi:10.2147/IJN.S247088
- Toledano M, Toledano-Osorio M, Osorio R, et al. Zinc Loaded Silica-Nanofibrous Polymers as Biomaterials for Bone Regeneration. *Polymers.* 2020;12.
- Liu L, Jin R, Duan J, et al. Bioactive iron oxide nanoparticles suppress osteoclastogenesis and ovariectomy-induced bone loss through regulating the TRAF6-p62-CYLD signaling complex. *Acta Biomaterialia.* 2020;103:281–292.
- Lavanya K, Chandran SV, Balagangadharan K, Selvamurugan N. Temperature- and pH-responsive chitosan-based injectable hydrogels for bone tissue engineering. *Materials Sci Eng.* 2020;111:110862.
- Gashtasbi F, Hasannia S, Hasannia S, Mahdi Dehghan M, Sarkarat F, Shali A. Comparative study of impact of animal source on physical, structural, and biological properties of bone xenograft. *Xenotransplantation.* 2020;e12628.
- Chen Y, Li W, Zhang C, Wu Z, Liu J. Recent Developments of Biomaterials for Additive Manufacturing of Bone Scaffolds. *Adv Healthcare Mater.* 2020;e2000724.
- Gronbach L, Wolff C, Klinghammer K, et al. A multilayered epithelial mucosa model of head neck squamous cell carcinoma for analysis of tumor-microenvironment interactions and drug development. *Biomaterials.* 2020;258:120277.
- He F, Springer NL, Whitman MA, et al. Hydroxyapatite mineral enhances malignant potential in a tissue-engineered model of ductal carcinoma in situ (DCIS). *Biomaterials.* 2019;224:119489.
- Zhang M, Shi J, Xie M, et al. Recapitulation of cartilage/bone formation using iPSCs via biomimetic 3D rotary culture approach for developmental engineering. *Biomaterials.* 2020;260:120334.
- Lu Y, Li L, Lin Z, et al. Modality for Rheumatoid Arthritis: combined Photothermal and Photodynamic Therapy Using Cu_{7.2} S₄ Nanoparticles. *Adv Healthcare Mater.* 2018;7:e1800013.
- Li Y, Jahr H, Zhou J, Zadpoor AA. Additively manufactured biodegradable porous metals. *Acta Biomater.* 2020;115:29–50.
- Liu DD, Zhang JC, Zhang Q, Wang SX, Yang MS. TGF-beta/BMP signaling pathway is involved in cerium-promoted osteogenic differentiation of mesenchymal stem cells. *J Cell Biochem.* 2013;114:1105–1114. doi:10.1002/jcb.24451
- Nie H, Wang CH. Fabrication and characterization of PLGA/HAP composite scaffolds for delivery of BMP-2 plasmid DNA. *J controlled release.* 2007;120:111–121.
- Hou LT, Tsai AY, Liu CM, Feng F. Autologous transplantation of gingival fibroblast-like cells and a hydroxylapatite complex graft in the treatment of periodontal osseous defects: cell cultivation and long-term report of cases. *Cell Transplantation.* 2003;12:787–797. doi:10.3727/000000003108747262
- Henkel KO, Gerber T, Dorfling P, et al. Stimulating regeneration of bone defects by implantation of bioceramics and autologous osteoblast transplantation. *MKG.* 2002;6:59–65.
- Radwan NH, Nasr M, Ishak RAH, Abdeltawab NF, Awad GAS. Chitosan-calcium phosphate composite scaffolds for control of post-operative osteomyelitis: fabrication, characterization, and in vitro-in vivo evaluation. *carbohydrate Polymers.* 2020;244:116482.
- Sadeghianmaryan A, Naghieh S, Alizadeh Sardroud H, et al. Extrusion-based printing of chitosan scaffolds and their in vitro characterization for cartilage tissue engineering. *Int J Biol Macromol.* 2020;164:3179–3192. doi:10.1016/j.ijbiomac.2020.08.180
- Lastra ML, Gomez Ribelles JL, Cortizo AM. Design and characterization of microspheres for a 3D mesenchymal stem cell culture. *Coll Surfaces B.* 2020;196:111322.
- Ansari Z, Kalantar M, Soriente A, et al. In-Situ Synthesis and Characterization of Chitosan/Hydroxyapatite Nanocomposite Coatings to Improve the Bioactive Properties of Ti6Al4V Substrates. *Materials.* 2020;13.
- Porwal K, Pal S, Dev K, et al. Guava fruit extract and its triterpene constituents have osteoanabolic effect: stimulation of osteoblast differentiation by activation of mitochondrial respiration via the Wnt/beta-catenin signaling. *J Nutritional Biochem.* 2017;44:22–34.
- Li Q, Fan YS, Gao ZQ, Fan K, Liu ZJ. Effect of Fructus Ligustri Lucidi on osteoblastic like cell-line MC3T3-E1. *J Ethnopharmacology.* 2015;170:88–95.
- Lee SU, Park SJ, Kwak HB, Oh J, Min YK, Kim SH. Anabolic activity of ursolic acid in bone: stimulating osteoblast differentiation in vitro and inducing new bone formation in vivo. *Pharmacol Res.* 2008;58:290–296.
- Tan H, Zhao C, Zhu Q, et al. Ursolic Acid Isolated from the Leaves of Loquat (*Eriobotrya japonica*) Inhibited Osteoclast Differentiation through Targeting Exportin 5. *J Agr Food Chem.* 2019;67:3333–3340.
- Jiang C, Xiao F, Gu X, et al. Inhibitory effects of ursolic acid on osteoclastogenesis and titanium particle-induced osteolysis are mediated primarily via suppression of NF-kappaB signaling. *Biochimie.* 2015;111:107–118.
- Peng M, Qiang L, Xu Y, Li C, Li T, Wang J. Modification of Cysteine 179 in IKKbeta by Ursolic Acid Inhibits Titanium-Wear-Particle-Induced Inflammation, Osteoclastogenesis, and Hydroxylapatite Resorption. *Mol Pharmaceutics.* 2018;15:5244–5251. doi:10.1021/acs.molpharmaceut.8b00747
- Ge YW, Lu JW, Sun ZY, et al. Ursolic acid loaded-mesoporous bioglass/chitosan porous scaffolds as drug delivery system for bone regeneration. *Nanomedicine.* 2019;18:336–346.
- Szewczyk A, Skwira A, Konopacka A, Sadej R, Walker G, Prokopowicz M. Mesoporous silica pellets as bifunctional bone drug delivery system for cefazolin. *Int J Pharmaceutics.* 2020;588:119718.

31. Li C, Qin W, Lakshmanan S, Ma X, Sun X, Xu B. Hydroxyapatite based biocomposite scaffold: a highly biocompatible material for bone regeneration. *Saudi J Biol Sci.* 2020;27:2143–2148.
32. Carvalho Vasconcelos R, Ferreira C, de Araujo EM, et al. Zirconia/hydroxyapatite (80/20) scaffold repair in critical size calvarial defect increased FGF-2, osteocalcin and OPG immunostaining and IL-10 levels. *Am J Translational Res.* 2020;12:2439–2450.
33. Pitaloka DAE, Cooper AM, Artarini AA, Damayanti S, Sukandar EY. Regulation of mitogen-activated protein kinase signaling pathway and proinflammatory cytokines by ursolic acid in murine macrophages infected with *Mycobacterium avium*. *Infect Dis Rep.* 2020;12:8717.
34. Deciga-Campos M, Cortes A, Pellicer F, Diaz-Reval I, Gonzalez-Trujano ME. Isobolographic analysis of the antinociceptive interaction between ursolic acid and diclofenac or tramadol in mice. *Planta Medica.* 2014;80:139–145.
35. Wang C, Gao Y, Zhang Z, et al. Ursolic acid protects chondrocytes, exhibits anti-inflammatory properties via regulation of the NF-kappaB/NLRP3 inflammasome pathway and ameliorates osteoarthritis. *Biomed Pharmacother.* 2020;130:110568.
36. Qian W, Li X, Shen L, et al. Antibacterial and antibiofilm activity of ursolic acid against carbapenem-resistant *Enterobacter cloacae*. *J Biosci Bioeng.* 2020;129:528–534. doi:10.1016/j.jbiosc.2019.11.008
37. Ahn YJ, Wang L, Foster S, Asmis R. Dietary 23-Hydroxy Ursolic Acid Protects Against Diet-Induced Weight Gain and Hyperglycemia by Protecting Monocytes and Macrophages Against Nutrient Stress-Triggered Reprogramming and Dysfunction and Preventing Adipose Tissue Inflammation. *J Nutritional Biochem.* 2020;108483.

International Journal of Nanomedicine

Dovepress

Publish your work in this journal

The International Journal of Nanomedicine is an international, peer-reviewed journal focusing on the application of nanotechnology in diagnostics, therapeutics, and drug delivery systems throughout the biomedical field. This journal is indexed on PubMed Central, MedLine, CAS, SciSearch®, Current Contents®/Clinical Medicine,

Journal Citation Reports/Science Edition, EMBase, Scopus and the Elsevier Bibliographic databases. The manuscript management system is completely online and includes a very quick and fair peer-review system, which is all easy to use. Visit <http://www.dovepress.com/testimonials.php> to read real quotes from published authors.

Submit your manuscript here: <https://www.dovepress.com/international-journal-of-nanomedicine-journal>